

LOUDSPEAKER ACOUSTIC FIELD CALCULATIONS WITH APPLICATION TO DIRECTIONAL RESPONSE MEASUREMENT

David W. Guinness and Ryan J. Mihelich

Eastern Acoustic Works, Inc.
1 Main St., Whitinsville, MA 01588 USA
PH: 508-234-6158 FAX: 508-234-6479
e-mail: david.gunness@eaw.com and ryan.mihelich@eaw.com

ABSTRACT

The traditional method of predicting the acoustical field produced by an arbitrarily shaped source is a high frequency, angle-limited reduction of the Kirchhoff-Helmholtz equation. The broad band, broad angle version of the Kirchhoff-Helmholtz equation is derived, and implemented as a numerical method. Acoustical field predictions of real sources developed with this method agree closely with measured data. This agreement even extends to low frequencies and angles near and beyond 90 degrees off of the primary axis. Applications of the technique are described, including a powerful and efficient directional response characterization method.

0 INTRODUCTION

"Point source approximation" is a phrase that has been common in the audio engineering field for over 100 years. In the decades leading to the publication of Theory of Sound, Part 2, in 1896 [1], Lord Rayleigh sought to evaluate the directionality of an aperture in a "plane screen." Certain simplifying assumptions were necessary to reduce the equations to a solvable form. Rayleigh assumed that the pressure magnitude and phase were both constant across the aperture, and that the "directivity pattern" could be assessed by treating the source aperture as an array of simple point sources. The solution to this simplified problem had already been demonstrated in the field of optics.

Sixty years later Harry Olson published Acoustical Engineering [2], including numerous graphs of "directional characteristics." The data for these graphs were generated using Rayleigh's procedure, and have come to be accepted as gospel by practitioners in the field - despite the fact that real devices differ from these approximations in important ways.

While Rayleigh's simplifying assumptions were expedient and warranted in 1896, there is no longer any reason to perpetuate them. The computing power available on every engineer's desktop is more than adequate for solving these problems numerically in their complete form. The necessary equations, known as Kirchhoff-Helmholtz (K-H) Integrals, are well known in other branches of acoustics and are presented authoritatively in general acoustics textbooks [3,4,5]. While point source approximations suggest the general directional characteristics of real devices, they consistently err in sometimes surprising ways.

Our work in this area was motivated by a desire to capture the complex directional behavior of horns, to be used in predicting their interactions. A paper delivered at the 107th A.E.S. Convention, *Improved Loudspeaker Array Modeling* by Guinness & Hoy [6], presented a promising technique for capturing a horn's behavior with a tessellation of its mouth. In order to improve the accuracy of this method and allow it to be extended to three-dimensional space, we needed to consider the full K-H Integral. A new installment of that paper, *Improved Loudspeaker Array Modeling - Part 2* [7], presents an expanded technique based on the full equation.

As the details of tessellation with the full K-H Integral became clear, we realized that the technique could also be useful as a general directional characterization process. The predominant form of measurement and modeling of commercial loudspeakers is a simplistic data-table procedure. This process is rife with error mechanisms and pitfalls; all growing out of its assumption that the far-field response is an attenuated and delayed version of the "medium-field" response. A measurement process based on a tessellated sphere would be immune from all of the error mechanisms that have been identified.

The spherical measurement technique will be dealt with briefly here, and the horn modeling technique is dealt with in depth in [6,7]. The primary focus of the current paper is to present the full K-H Integral in detail, including its application to tessellation.

1 THE KIRCHHOFF-HELMHOLTZ INTEGRAL EQUATION

Kirchhoff's scalar diffraction theory "uses Green's theorem to express a scalar field inside a closed volume, V in terms of the values of the field and the normal derivative of the field on the boundary surface, S ." [8] The scalar field, $p(\mathbf{x},t)$ is to have harmonic time dependence and is to satisfy the Helmholtz wave equation inside V .

Green's theorem is given by Equation 1.

$$\int_V (G \nabla^2 p - p \nabla^2 G) d^3x = \oint_S \left(G \frac{\partial p}{\partial n} - p \frac{\partial G}{\partial n} \right) da \quad (1)$$

G is the free space Green's function, $G(\mathbf{x},\mathbf{x}')$ satisfying Equation 2, and p is the scalar field, $p(\mathbf{x},t)$.

$$(\nabla^2 + k^2)G(\mathbf{x},\mathbf{x}') = -\delta(\mathbf{x} - \mathbf{x}') \quad (2)$$

The free space Green's function is given by,

$$G(\mathbf{x},\mathbf{x}') = R^{-1} e^{jkR}$$

the gradient of this Green's function is,

$$\nabla G(\mathbf{x},\mathbf{x}') = \frac{\mathbf{e}_R}{R^2} (jkR - 1) e^{jkR}$$

Substituting these values into Equation 1 gives Equation 3.

$$\hat{p}(\mathbf{x}) = \frac{1}{4\pi} \oint_S G(\mathbf{x}, \mathbf{x}') [\nabla \hat{p}(\mathbf{x}') + \hat{p}(\mathbf{x}') (jk - 1/R) \mathbf{e}_R] \cdot \mathbf{n}_S dS \quad (3)$$

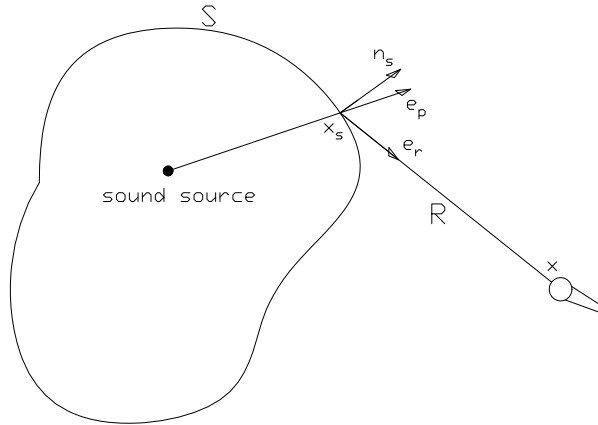


Figure 1: Definition of Terms

In Equation 3, the integration is carried out over an arbitrary surface, S , enclosing the sources and another surface, S_∞ that can be taken to be "at infinity." Since the fields in this problem are taken to originate inside a surface that completely encloses the sources as shown in Figure 1, all waves are outgoing towards S_∞ . The Sommerfeld radiation condition is then applied - that the wave must vanish at least as fast as the inverse of the radius, as the radius goes to infinity. It can therefore be assumed that the integration in Equation 3 is carried out only over the surface, S , containing the sources. The Kirchhoff-Helmholtz Integral Theorem is the result and is presented as Equation 4.

$$\hat{p}(\mathbf{x}) = \frac{1}{4\pi} \iint \frac{1}{R} e^{jkR} [\nabla \hat{p}(\mathbf{x}_s) + \hat{p}(\mathbf{x}_s) (jk - 1/R) \mathbf{e}_R] \cdot \mathbf{n}_S dS \quad (4)$$

This equation is used to predict the spatial pressure response based on a pressure and normal pressure gradient map of a surface, S . Since the pressure gradient is proportional to velocity, pressure and its gradient may not be specified arbitrarily. For one pressure field there exists a unique velocity (pressure gradient) field related by radiation impedance.

1.1 The Gradient Term

Other useful forms of this integral may be derived that are appropriate for specific applications. As a measurement tool for instance, one may wish to measure the spherical polar response of a loudspeaker and use that spherical data to create a tessellated model of the mapped surface. One may also wish to use a form of Equation 4 that is better suited for horn synthesis or analysis. Both of these applications are examples where tessellation would be used. A form of Equation 4 that is useful for tessellation is presented in Equation 5. This equation predicts the pressure at any point in space from a single tessella. The θ_x and θ_y terms in Equation 5 represent the horizontal and vertical wavefront curvature in terms of the included angle of each arc. The low frequency divergence can be derived in terms of the included angles, and the propagation angle, θ_p .

$$p(\mathbf{x}) = \frac{1}{4\pi} \iint \frac{1}{R} e^{jkR} \hat{p}(\mathbf{x}_s) \left[(\mathbf{e}_R \cdot \mathbf{n}_s) + \cos(\theta_p) + \frac{\cos(\theta_p)}{jk} \left(\frac{\sin(\theta_y/2)}{y} + \frac{\sin(\theta_x/2)}{x} \right) \right] dS \quad (5)$$

For the spherical measurement technique, a simplified method may be used in circumstances when the source is reasonably close to the center of the measurement sphere. This form is presented as Equation 6 where r_d is the radius of the measurement sphere.

$$p(\mathbf{x}) = \frac{1}{4\pi} \iint \frac{1}{R} e^{jkR} \hat{p}(\mathbf{x}_s) \left[(\mathbf{e}_R \cdot \mathbf{n}_s) + 1 + \frac{j}{kr_d} \right] dS \quad (6)$$

1.2 Illustrative Examples

It is instructive to show practical applications of the Kirchhoff-Helmholtz Integral. Interesting examples that cannot be solved correctly using traditional methods can be solved using this method. Direct radiating low frequency devices can be modeled more accurately than with point source methods. A point source within a spherical surface will be used as a demonstration of a simple case that is incorrectly represented by a point source approximation, but correctly represented by the full K-H integral.

1.2.1 Directional Response of Low Frequency Devices

The K-H integral will predict the off axis response of direct radiating loudspeakers at moderately low frequencies with greater accuracy than the traditional method. Measured data exhibits approximately 6dB more attenuation at 90° off axis than the point source method predicts. The full K-H integral predicts an off-axis response that agrees with measurements.

Looking at the individual terms of the K-H integral gives insight into why this happens. The first term constitutes the "point source approximation", and is a monopole term resulting from the velocity. The second term, which includes $\bar{\mathbf{e}}_R \cdot \bar{\mathbf{n}}_s$, is a dipole term resulting from the pressure distribution. When added to the monopole term, it yields a cardioid pattern. There is also a low frequency term that eventually transitions the cardioid response to a monopole

response at very low frequencies, and a near field term which is negligible for distances which are large compared to the individual tessella dimensions.

The traditional method would predict directional response based on the monopole term only, giving low-frequency results that are known to be approximately 6dB in error at 90° off axis. While the new method still does not provide exact results in the back hemisphere, it does provide very precise agreement with measured data over the front hemisphere.

1.22 Point Source Centered in a Sphere

It is common to assume that a far field prediction point can be taken as a delayed and attenuated version of a measured medium-field response in the same direction. This assumption is only true for a point source located at the point of rotation. Since all real sources have finite dimensions, the assumption is rarely valid in actual practice. The magnitude & phase response will be affected by various geometrical error mechanisms (discussed in Section 3), and the phase response will be progressively more errant at points away from the original measurement point. The Kirchhoff-Helmholtz integral theorem teaches how to solve these problems: we must integrate the complex pressure over a complete surface surrounding the source.

As a simple example of the concepts presented thus far, consider a sphere of radius R surrounding a point source of unity strength¹ located at the center of the sphere. The pressure will be constant over the surface of the sphere. Suppose now that the nature of the source is unknown. The pressure on the surface of the sphere will be used to predict the pressure at a point, \mathbf{x}_o , in the space outside the sphere.

Using traditional point source methods for modeling the sphere, the pressure calculated for \mathbf{x}_o will be incorrect. This can most easily be illustrated by the impulse response calculated at \mathbf{x}_o , which is shown in Figure 2a. In addition to the expected impulse arrival from the front of the sphere, a second impulse arrival is predicted, which originates at the far side of the sphere. This result is obviously incorrect.

¹ The source has been low-pass filtered to broaden the pulse for improved clarity in Figures 2a,b, & c.

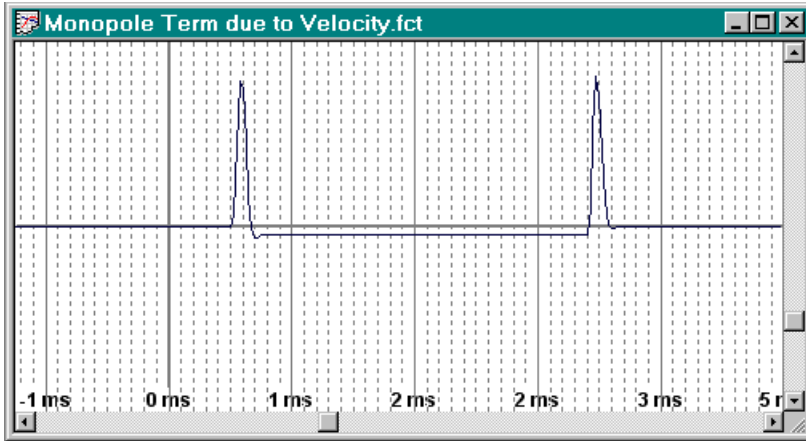


Figure 2a: Impulse Response of Spherical Source - Velocity Term

The full K-H integral has two additional terms that eliminate this discrepancy. The dipole term produces the impulse response shown in Figure 2b. Its leading impulse is identical to that of the monopole term, but its trailing impulse is inverted (because $\vec{e}_R \cdot \vec{n}_S$ is -1 at 180°). When the dipole term is added to the monopole term, the trailing impulse is cancelled - leaving only the expected impulse (with its magnitude doubled) and a wide, rectangular, negative going impulse.

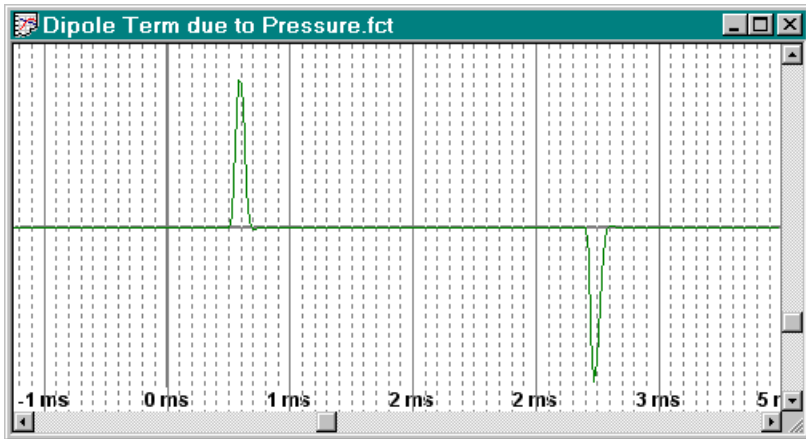


Figure 2b: Impulse Response of Spherical Source - Pressure Term

The divergence term produces the impulse response shown in Figure 2c. This term perfectly cancels the negative-going rectangle which is part of the monopole term. The net response is the expected perfect impulse.

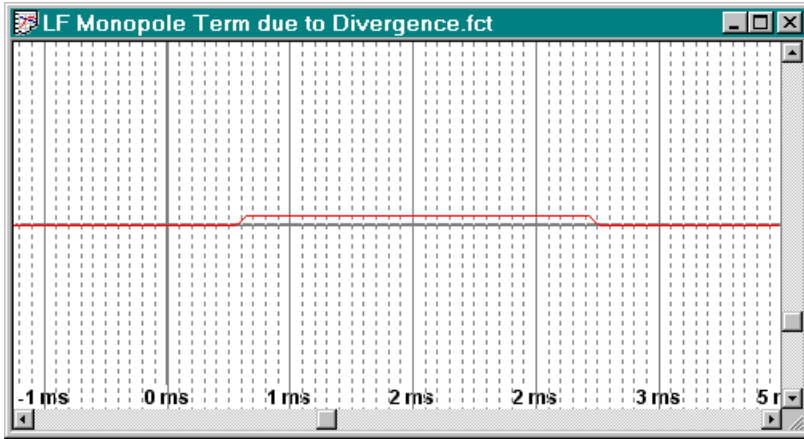


Figure 2c: Impulse Response of Spherical Source - Divergence Term

1.3 Tessellation

The derivation of Equations 4-6 is useful for the prediction of the acoustical field produced by a single tessella. To be useful in practical applications, a surface must be tessellated. Application of this technique is a boundary element method that requires the surface² to be divided into geometrical shapes creating a mesh. The most common surfaces are the sphere and the finite plane. The most common geometrical shapes to create the mesh are the rectangle, the trapezoid, and the triangle.

Taking Equation 5 as the master equation for tessellation and applying it to a tessellated surface yields a sum of surface integrals. Each surface integral represents a single tessella on the surface that can be of arbitrary shape and size and can have any complex pressure distribution across it. This summation, presented as Equation 7, must be numerically implemented and solved by a computer. The summation here is over the n tessellae that make up the complete surface.

$$p(\mathbf{x}) = \sum_n \frac{1}{4\pi} \iint \frac{1}{R} e^{jkR} \hat{p}(\mathbf{x}_s) \left[(\mathbf{e}_R \cdot \mathbf{n}_s) + \cos(\theta_p) + \frac{\cos(\theta_p)}{jk} \left(\frac{\sin(\theta_y/2)}{y} + \frac{\sin(\theta_x/2)}{x} \right) \right] dS \quad (7)$$

The result is a complex pressure that is solved for a single point in space and a single frequency. This greatly reduces computation time, it is not necessary to calculate pressures over a complete surface as in the Fourier [5] nor boundary element methods or a complete volume as in finite element methods [9].

1.3.1 Tessella Directivity Equations

The standard equations that describe the radiation pattern from a planar source [2,10] are based on the assumption that wave propagation is normal to that source. While this is a valid

² In this context the surface is defined as the surface over which pressure measurements were made.

assumption for many wave problems, there are instances when we wish to include non-uniform distribution of magnitude and/or phase on the surface. In addition, the literature describes only rectangular and circular surfaces. It is also desired to introduce tessellae that can take the shape of an arbitrary trapezoid³ to improve results when tessellating surfaces such as spheres.

1.3.2 Non-normal Propagation Through a Tessella

Including non-normal propagation in the tessella model requires a reconsideration of Rayleigh's integral [3,5] using a non-uniform complex pressure distribution over the surface of integration. While the magnitude can be taken as constant, the phase varies linearly (pure delay) over the surface of the tessella. This represents a tessella with non-normal propagation angle, $\bar{\mathbf{e}}_p$ through the surface. This system can be represented by Equation 8. If the magnitude were to vary over the surface, additional terms would be required.

$$\hat{p}(\mathbf{x}) = \hat{p}_0 \text{Exp}(jk(y\bar{\mathbf{e}}_p \cdot \bar{\mathbf{y}} + z\bar{\mathbf{e}}_p \cdot \bar{\mathbf{x}})) \quad (8)$$

Using Equation 8 leads to a slightly different directivity formula from that of a simple rectangular surface as presented in Olson. For the rectangular surface with skewed propagation per Equation 8, the directivity pattern is given by Equation 9.

$$p(\bar{\mathbf{e}}_R) = 4lw \text{Sinc}(m_y + k_y) \text{Sinc}(m_z + k_z) \quad (9)$$

where,

$$k_y = 2\pi/\lambda \sin(\bar{\mathbf{e}}_R \cdot \bar{\mathbf{y}})$$

$$k_z = 2\pi/\lambda \sin(\bar{\mathbf{e}}_R \cdot \bar{\mathbf{z}})$$

In Equation 9, m_y and m_z are the slope of the plane in the y and z directions respectively, the normal of which is in the direction of propagation, $\bar{\mathbf{x}}$. Referring to Figure 1, $m_y = \bar{\mathbf{e}}_p \cdot \bar{\mathbf{y}}$ and $m_z = \bar{\mathbf{e}}_p \cdot \bar{\mathbf{z}}$.

It may be desirable to represent spherical variations in arrival time, for tessellating a sphere or representing a curved wavefront. Using this method eliminates the problem of concentrated high frequency beams on the axis of each flat tessella. To account for wavefront curvature, we once again adjust our expression for the complex pressure over the tessella:

$$\hat{p}(\mathbf{x}) = \hat{p}_0 \text{Exp}\left(jk\left[y\bar{\mathbf{e}}_p \cdot \bar{\mathbf{y}} + z\bar{\mathbf{e}}_p \cdot \bar{\mathbf{z}} + \left(\sqrt{r_y^2 + y^2} - r_y\right) + \left(\sqrt{r_z^2 + z^2} - r_z\right)\right]\right) \quad (10)$$

We know of no closed-form solution to the resulting Fourier integral. Consequently, the expression must be numerically integrated.

³ A triangle is a reduction of the trapezoidal equation.

1.3.3 The Trapezoidal Tessella Equation

As mentioned above, it is useful to define a non-rectangular tessella to aid in the tessellation of non-rectangular surfaces. When tessellating a sphere for instance, triangles are useful near the poles. Trapezoids are also necessary to avoid overlap on spheres. A single equation describes the normal radiation through a rectangular, triangular or trapezoidal tessella. Equation 11 results from the application of the two-dimensional Fourier Transform of this surface.

$$p(\bar{\mathbf{e}}_R) = \frac{1}{jk_z} \left[\frac{\text{Exp}(j(k_y y + k_z y m_1 + k_z b_1))}{j(k_y + k_z m_1)} - \frac{\text{Exp}(j(k_y y + k_z y m_2 + k_z b_2))}{j(k_y + k_z m_2)} \right]_{-y_1}^{y_1} \quad (11)$$

This equation allows complete flexibility to create any trapezoidal source by simply substituting values for the line equations, $y = m_1 x + b_1$ and $y = m_2 x + b_2$, that define the non-parallel sides. The most commonly needed sources do not require as much flexibility as Equation 11 allows. Tessellation of a sphere for instance requires only isosceles triangles and isosceles trapezoids.

2 APPLICATION TO LOUDSPEAKER MEASUREMENT

The Kirchhoff-Helmholtz integral theorem gives us a methodology for predicting the far-field pressure given a mapping of the near-field pressure. The acquisition of pressure over a completely enclosing surface is not a trivial exercise, but one that has already been undertaken by most professional loudspeaker manufacturers in order to obtain spherical response data. In the case of horns, the mapping need only cover the mouth of the horn, since the acoustic output of the back surface of the horn can be taken to be zero. Characterization of horn directionality is covered in some detail in [5,6].

For a completely enclosing mapping surface, an obvious choice is a sphere. Two potential applications of spherical sampling are evident: Broad-band, high precision directional response characterization, and high-resolution low-frequency response measurement in reflective rooms.

2.1 Directional Response Characterization

Traditional loudspeaker measurement techniques give a spherical polar response of the loudspeaker under test with some angular resolution (usually 5°). The resulting data table can then be used in modeling programs to predict the response of the loudspeaker in a room. The process is fraught with errors, as documented by Ureda [11] and Guinness [12]. A tessellated spherical model, on the other hand, is immune to geometric errors.

2.1.1 Geometric Errors

Geometric errors result whenever the size of a source is significant relative to the microphone distance. If the apex of the walls of a horn do not converge at the point of rotation, the shape of the polar magnitude response will be distorted. Furthermore, even if the apex is at the point of

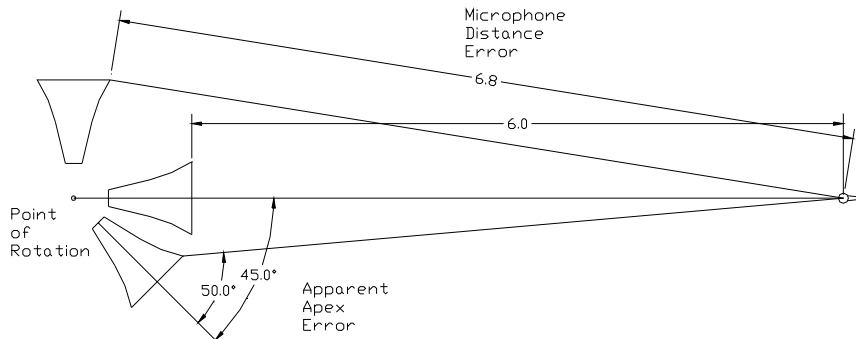


Figure 3: Geometric Errors

rotation, there will still be an apparent apex error when the horn is rotated beyond its coverage angle. Any source of finite extent is subject to these geometric errors. Careful placement of the loudspeakers cannot solve this problem, since the apexes of the horizontal and vertical sections rarely coincide. In fact, the effective location of the apex may change with frequency.

2.1.2 Phase Response

Recently, polar phase response has received considerable attention [13], as practitioners desire to examine the combinational behavior of loudspeakers. The various geometric errors have been discussed in the literature in terms of their effect on magnitude response, but it should be obvious that these errors also affect the phase response. In fact, phase response is much more sensitive to geometric errors than magnitude response. With a measurement distance of 6 m, a 0.72 m distance discrepancy is required to produce a 1 dB magnitude error. However, for accurate array calculations at 8 kHz, the arrival path must be accurate to within about 10 mm.

2.1.3 Interpolation Errors

Interpolation errors arise when modeling software requires the response at a point in space where no measurement was taken. If 5° resolution data was obtained and a 12.5° response is requested, interpolation must take place. Since nothing is known about the source other than its response at the sample angles, the modeling program cannot necessarily interpolate the complex response correctly. The problem is particularly severe when the arrival time varies by

1/2 period or more from one sampled point to the next - a condition that is not unusual at high frequencies. When this occurs, interpolation is problematic due to the wrapping of the phase.

With a tessellated model, on the other hand, there are no "interpolated" observation positions - since the response at any point depends on all the tessellae.

2.1.4 Variation of the Speed of Sound

The speed of sound varies by 1% if the temperature varies by about 6°C. In order to obtain measurements of disparate loudspeakers at 6 m with an arrival time accuracy equivalent to 10 mm of propagation (allowing interference calculations at 8 kHz), the temperature would have to be controlled (or recorded) within 1°C. Clearly, the shorter the measurement distance, the less sensitivity there will be to environmental variations. If the temperature is recorded at the time of measurement, a tessellated model can be used to make accurate predictions of interactions between loudspeakers measured under different atmospheric conditions.

2.2 Low Frequency Response in Reflective Rooms

The problems associated with obtaining accurate low frequency response in reflective rooms are well known. Near-field measurements minimize the effect of reflections from nearby surfaces and give the approximate shape of the low-frequency response. A method originated by Keele [14] uses the enclosure's internal pressure response and volume to estimate the power response of a direct radiating woofer. However, both of these methods negate the directionality of the source, and neither is effective for bass horns.

A near-field spherical pressure map may be obtained by measuring an elevated loudspeaker. This minimizes the effect of nearby surfaces (e.g., the floor). Using the tessellated model to calculate the far-field response then accurately accounts for source directionality. The result is the best-possible estimate of far-field anechoic response.

3 CONCLUSIONS

The Kirchhoff-Helmholtz Integral was proposed as a practical and powerful replacement for the traditional point source approximation. Several forms of the equations were presented, each appropriate to a different use.

Several applications of the equations were presented, including loudspeaker synthesis, measurement, and modeling. The calculations are more involved than the traditional method, but are well within the capabilities of current desktop computers.

REFERENCES

- [1] Lord Rayleigh, *Theory of Sound, Vol. II*, MacMillan & Co., London, 1896
- [2] H. F. Olson, *Elements of Acoustical Engineering*, Van Nostrand, New York, 1947

- [3] Allan D. Pierce, *Acoustics, An Introduction to its Physical Principles and Applications*, Acoustical Society of America, 1989.
- [4] P. Filippi, D. Habault, J.P. Lefebvre, A. Bergassoli, *Acoustics, Basic physics, theory and methods*, Academic Press, 1999
- [5] Earl G. Williams, *Fourier Acoustics, Sound Radiation and Nearfield Acoustical Holography* Academic Press, 1999
- [6] D.W. Guinness, and W.R. Hoy, "Improved Loudspeaker Array Modeling," presented at the 107th Convention of the Audio Engineering Society, 1999, Preprint #5020
- [7] D.W. Guinness and W.R. Hoy, "Improved Loudspeaker Array Modeling - Part 2," presented at the 109th Convention of the Audio Engineering Society, 2000
- [8] John D. Jackson, *Classical Electrodynamics*, John Wiley & Sons, Inc., 1975
- [9] R. L. Ferrari, P. P. Silvester, *Finite Elements for Electrical Engineers*, Cambridge University Press, 1996
- [10] L. L. Beranek, *Acoustics* (McGraw-Hill, New York, 1954).
- [11] M. S. Ureda, "Apparent Apex Theory," presented at the 61st Convention of the Audio Engineering Society, 1978, Preprint #1403.
M. S. Ureda, "Apparent Apex Revisited", 1991, Preprint #3040.
M. S. Ureda, "Apparent Apex, Part III: The Three-Dimensional Case", 1991, Preprint #3166.
M. S. Ureda, "Apparent Apex, Part IV: Direct Radiators", 1992, Preprint 3324.
M. S. Ureda, "Apparent Apex", 1997, Preprint #4467.
- [12] D. W. Guinness, "Loudspeaker Directional Response Measurement," presented at the 89th Convention of the Audio Engineering Society, 1990, Preprint #2987.
- [13] W. Ahnert, J. Baird, S. Feistel, P. Meyer, "Accurate Electroacoustic Prediction utilizing the Complex Frequency Response of Far-Field Polar Measurements," presented at the 108th Convention of the Audio Engineering Society, 2000, Preprint #5129
- [14] D. B. Keele, "Low-Frequency Loudspeaker Assessment by Nearfield Sound-Pressure Measurement," *J. Audio Eng. Soc.*, Vol. 22, Number 3 pp. 154 (1974)